JOURNAL OF AIRCRAFT
Vol. 43, No. 4, July–August 2006

Effect of Injection Slot Size on the Performance of Coflow Jet Airfoil

Ge-Cheng Zha,* Craig D. Paxton,† and Clark A. Conley‡
University of Miami, Coral Gables, Florida 33124
and
Adam Wells§ and Bruce F. Carroll‖
University of Florida, Gainesville, Florida 32611-6250

DOI: 10.2514/1.16999

Two coflow jet airfoils with injection slot size differing by a factor of 2 are tested in a wind tunnel to study the effect of injection slot size. At the same angle of attack, the larger injection slot size airfoil passes about twice the jet mass flow rate of the smaller injection slot size airfoil. The smaller injection slot size airfoil is more effective in increasing the stall margin and maximum lift, whereas the larger slot coflow jet airfoil is more effective in reducing drag. To achieve the same lift, the smaller injection slot size airfoil has much less energy expenditure than the larger injection slot airfoil. A coefficient of jet kinetic energy is introduced, which appears to correlate well with the maximum lift and stall margin when coflow jet airfoil geometry varies. Both the jet kinetic energy coefficient and the momentum coefficient correlate well with drag reduction. No optimization of the airfoil configuration is pursued in this research, and the results indicate that there is a great potential for coflow jet airfoil performance improvement.

Nomenclature

A	=	area
A^*	=	choked area
C	=	discharge coefficient
C_D	=	drag coefficient
C_L	=	lift coefficient
C_μ	=	momentum coefficient
c_t	=	specific fuel consumption
D	=	pipe internal diameter
d	=	orifice diameter
k	=	turbulent kinetic energy
M	=	Mach number
$\dot{m}$	=	mass flow rate
n	=	number of samples
P_t	=	total pressure
p	=	static pressure
q_m	=	mass fow rate
R	=	universal constant
S	=	wing span area, $b \times$ chord
$S_{\text{injection slot}}$	=	slot area, slot height $\times$ slot width
T	=	static temperature
T_t	=	total temperature
t	=	student's t value for corresponding confidence level
U	=	velocity
V	=	velocity
y^+	=	nondimensional length scale for turbulent boundary layer
γ	=	ratio of specific heats
Δ	=	uncertainty
ϵ	=	gas expansion factor
ρ	=	density
σ	=	standard deviation

Presented as Paper 1260 at the AIAA the 43rd Aerospace Sciences Meeting and Exhibit Conference, Reno, NV, 10–13 January 2005; received 6 April 2005; revision received 18 November 2005; accepted for publication 24 December 2005.

*Associate Professor, Department of Mechanical and Aerospace Engineering; zha@apollo.eng.miami.edu. AIAA Member.
†Graduate Student, Department of Mechanical and Aerospace Engineering.
‡Senior Undergraduate Student, Department of Mechanical and Aerospace Engineering.
§Graduate Student, Department of Mechanical and Aerospace Engineering.
‖Associate Professor, Department of Mechanical and Aerospace Engineering. AIAA Associate Fellow.

I. Introduction

TO improve aircraft performance, revolutionary technology should be pursued to dramatically reduce the weight and fuel consumption of the aircraft and to significantly increase aircraft mission payload and stall margin. Both military and commercial aircraft will benefit from this technology. Flow control is the most promising route to bring significant performance improvement to aircraft [1–7]. Recently, Zha and Paxton [8] and Zha et al. [9] have developed a new promising airfoil flow control technique using a coflow jet, which significantly increases lift, stall margin, and drag reduction.

The coflow jet airfoil is designed with an injection slot near the leading edge and a suction slot near the trailing edge on the airfoil suction surface. The slots are opened by translating a large portion of the suction surface downward. A high energy jet is injected tangentially near the leading edge in the same direction of the main flow, and the same amount of mass flow is drawn in near the trailing edge. The turbulent shear layer between the main flow and the jet causes strong turbulence diffusion and mixing under the severe adverse pressure gradient, which enhances the lateral transport of energy from the jet to the mainflow allowing the main flow to overcome the severe adverse pressure gradient and remain attached at high angle of attack. The high energy jet induces high circulation and hence generates high lift. The coflow jet (CFJ) airfoil can recirculate the jet mass flow and can significantly reduce the penalty to the propulsion system by avoiding dumping the jet mass flow or having zero net jet mass flow.

In [8,9], an overview of different flow control methods is given. The working mechanism of the CFJ airfoil is different from that of a circulation control (CC) airfoil [10,11]. A CC airfoil relies on a large leading edge (LE) or trailing edge (TE) to create the Coanda effect and enhance circulation. The large TE or LE may generate large drag during cruise. The CFJ airfoil relies on the wall jet mixing with the main flow to energize the main flow and overcome the adverse pressure gradient so that the flow can induce high circulation and remain attached at high AOA. The CC airfoil dumps away the jet mass flow, which is a considerable penalty to the propulsion system.

A CC airfoil without LE injection will reduce stall margin even though it increases lift [12]. Compared with synthetic jet flow control, the enhancement of airfoil performance by the CFJ airfoil is considerably better because the interaction of the synthetic jet with the main flow is weak [8,9,13]. The synthetic jet airfoil also exhibits little increase in stall margin [13]. The CFJ airfoil simultaneously achieves three crucial effects with low energy expenditure: lift enhancement, stall margin increase, and drag reduction.

The benefit of the high performance CFJ airfoil can be realized by integrating the airframe with the propulsion system so that the gain outweighs the cost of pumping and recirculating the coflow jet. To demonstrate this benefit, a preliminary conservative mission analysis of the military aircraft F-5E, assuming the CFJ airfoil is used, is conducted in [14], and a significant performance improvement is shown. In the mission analysis, the propulsion system costs an extra of 1.8% of energy expenditure to pump and recirculate the coflow jet. However, the gain from the airframe outweighs the penalty and results in a 9% reduction of fuel consumption. The endurance and range are increased by 38% and 41%, respectively. The V_{stall} is reduced by 44%, and the take off and landing distance is reduced by 68%.

An interesting feature of the CFJ airfoil is its supersuction at the leading edge, which produces such a low pressure at the LE that a thrust is generated. The contributions of the force in the streamwise direction due to jet injection and suction momentum are mostly canceled out by each other because the injection and suction flow rates are the same. The drag reduction mechanism of the CFJ airfoil, therefore, is not due to the momentum thrust from the jet. It is due to the large circulation induced by the coflow jet. A CFJ airfoil hence achieves a similar feature to that of a bird's flapping wing, which relies on the leading edge supersuction to generate thrust and high circulation to generate lift. The CFJ airfoil generates both lift and thrust with a fixed wing. This feature gives a new thrust component in the aircraft, which can rely less on the jet or fan thrust. The benefit is that it can reduce the jet velocity and therefore the jet noise that has eighth power dependence on the nozzle jet exhaust velocity.

Using both injection and suction in a CFJ airfoil has two advantages: 1) It strengthens the jet attachment to resist the severe adverse pressure gradient at high angles of attack to make the main flow attached. The study in [15] indicates that the airfoil with only the injection of the same strength and no suction generates lower lift enhancement and smaller drag reduction. The stall angle of attack is also less. 2) The suction provides the entrance for the jet recirculation to achieve zero net jet mass flow rate. The energy state at suction location is usually higher than that of the freestream. This also makes recirculating the jet flow more efficient than drawing the jet flow from the freestream.

The above advantages of the CFJ airfoil may derive the following superior aircraft performances: 1) extremely short distance for take off and landing; 2) supersonic aircraft with high subsonic performance; 3) high maneuverability, high safety, and fast acceleration of military aircraft; 4) very economic fuel consumption; 5) small wing span for easy storage, light weight, and reduced skin friction and form drag; and 6) low noise due to no high lift flap system and low nozzle jet velocity.

The CFJ airfoil concept is new and many issues of the working mechanism are not yet well understood. The turbulent mixing between the jet and the main flow that transfers energy from the jet to the main flow is the fundamental working principle [8]. The CFJ airfoil performance is more sensitive to the injection process than to the suction process [14]. The injection slot should be located as close to the leading edge as possible but should be located downstream of the suction peak. This is to ensure that the adverse pressure gradient after the suction peak enhances the wall jet mixing with the main flow [16].

The objective of this paper is to experimentally study the effect of injection slot size on the performance of the CFJ airfoil. The results of this paper show that the CFJ airfoil with different geometries can exhibit very different performance, which indicates that there are performance benefits to be gained through geometry optimization.

II. Coflow Jet Airfoil Geometry

Figure 1 shows the baseline airfoil, NACA0025, and two airfoils with coflow jet slots. The NACA0025 airfoil was selected as the baseline airfoil due to its large thickness to facilitate implementation of a coflow jet, internal ducts, and instrumentation. The CFJ airfoil concept also works very well for thin airfoils as shown by the CFD simulation [8,14]. The chord length of the airfoil is 0.1527 m and the span is 0.3 m. The coflow jet airfoils are defined using the following convention: CFJ4dig-INJ-SUC, where 4dig is the same as NACA 4 digit convention, INJ is replaced by the percentage of the injection slot size to the chord length, and SUC is replaced by the percentage of the suction slot size to the chord length. For example, the CFJ0025-065-196 airfoil has an injection slot height of 0.65% of the chord and a suction slot height of 1.96% of the chord. The new suction surface shape is a downward translation of the portion of the original suction surface between the injection and suction slot. The CFJ0025-131-196 is constructed in the same way by recessing the suction surface by 1.31% of the chord at the injection slot and 1.96% of the chord at the suction slot.

The CFJ0025-131-196 airfoil is designed with an injection slot size twice as large as that of the CFJ0025-065-196 airfoil to examine the effect of the injection slot size. The suction slot size is unchanged. The slot locations are also the same as those of the CFJ0025-065-196 airfoil. Previous studies [8,17] indicate that the suction slot size needs to be larger than the inlet slot size to ingest the same amount of jet mass flow without being choked. The injection and suction slots are located at 7.11% and 83.18% of the chord from the leading edge, respectively. The slot faces are normal to the suction surface to make the jet tangential to the main flow.

The internal ducts for both the injection and suction slots are also illustrated in Fig. 1, labeled as the high pressure and low pressure cavities. The high pressure flow is injected into the high pressure cavity and then passes through a block of Duocel aluminum foam. The Duocel foam acts as a baffle that gives a uniform flow

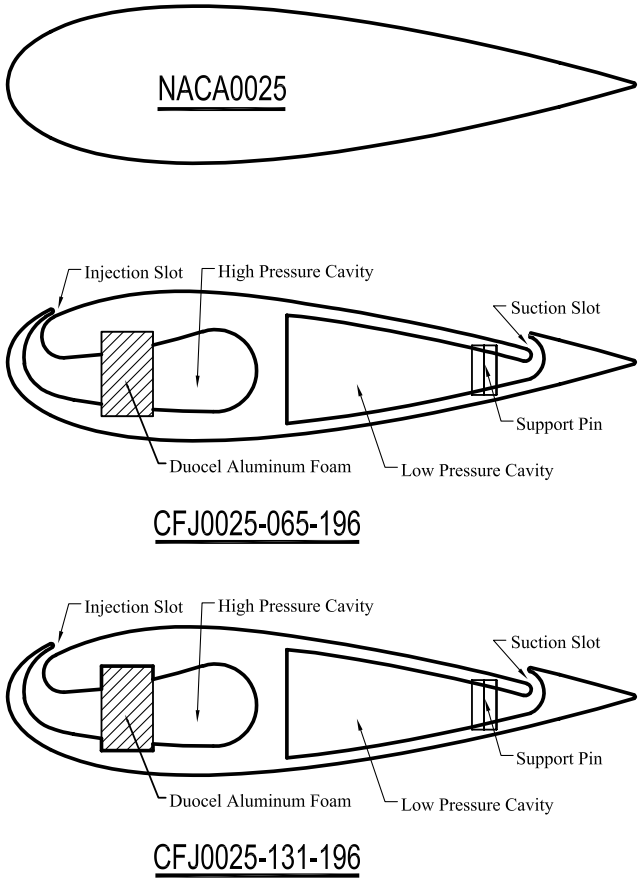

Fig. 1 The sections of baseline NACA0025, CFJ0025-065-196, and CFJ0025-131-196 airfoils.

distribution downstream of the foam and generates a highly uniform coflow jet, which is necessary to achieve two-dimensional flow for the CFJ airfoil testing. Computational fluid dynamics was used as a design tool to simulate the CFJ airfoils and their secondary flow ducts inside the wind tunnel. Very good two-dimensionality is achieved with the CFD analysis and is verified in the experiment. Both the injection and suction ducts are designed to have a continually converging or diverging shape to ensure that the throat is located at the injection and suctions slots. CFD results are used to verify that the injection and suction slots can pass the required mass flow rate of 0.1 kg/s under the experimental conditions.

III. Wind-Tunnel Measurement Setup

A. Wind Tunnel

The AEROLAB educational wind tunnel located at the University of Florida is used for this research. The test section of this tunnel is $12'' \times 12'' \times 24''$. A TSI, Inc., particle image velocimetry system is used for flow visualization and creating velocity vector fields on the midspan location. The lift, drag, and pitching moments are measured by strain gauges located on the sidewall sting tube.

The coflow jet is injected through the sting tube into the high pressure cavity and is drawn through a suction manifold on the opposite side of the airfoil, illustrated in Fig. 2. The injection system consists of a compressor and two large storage tanks that provide a continuous constant choked flow.

The airfoil is fixed on the sidewall sting on the injection side and is cantilevered on the suction side. Sufficient clearance is made between the cantilevered end and the wind-tunnel wall to prevent them from touching the wind-tunnel wall. A sealed Plexiglass box is mounted outside of the suction side wind-tunnel wall to prevent air leakage from the wind tunnel. The light weight and soft latex suction tubes minimize force translation and connect the suction system with the airfoil through the transparent Plexiglass box. This allows the particle image velocimetry camera to visualize and measure the flow velocity vector fields.

The external suction system consists of four 240 gal vacuum tanks, one 60 gal tank, one 80 gal tank, and two vacuum pumps. This system provides suction for 12–30 s within the required mass flow rate range.

B. Measurement Calibration

The airfoil lift and drag components are calibrated using a known weight at the center span of the airfoil in its test configuration with the latex tubes attached. This calibration showed a highly linear trend for both lift and drag with R^2 values of 0.9994 and 0.9995 [18], respectively. Using the student's t distribution, the uncertainty of lift and drag is given by [18]:

$$\Delta = \frac{t\sigma}{\sqrt{n}} \tag{1}$$

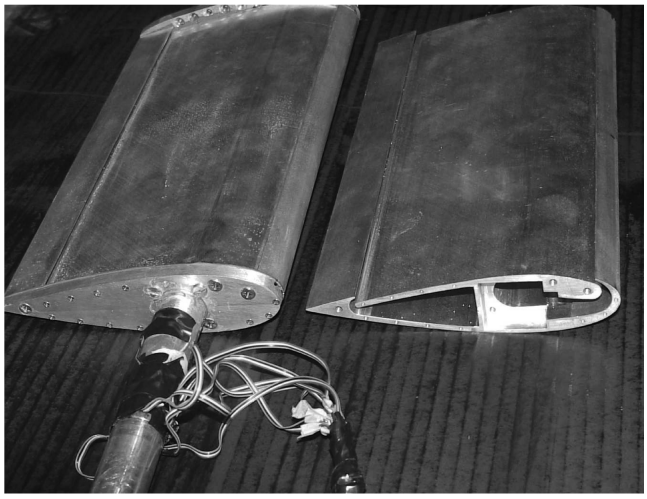

Fig. 2 The tested CFJ airfoils showing the injection side.

For a 95% confidence level and $n = 50$ samples, $t = 2.0105$.

The standard deviation ranges from 1 N at lower AOA to 5 N at higher AOA for both lift and drag. This corresponds to standard deviation in terms of C_L and C_D of 0.031–0.153. The uncertainty in C_L and C_D would thus be 0.008814 at lower AOA and 0.043 at higher AOA. Strain gauge measurements are taken at approximately 2/3 Hz. These single measurements are actually an average of five integrations of a digital signal with a two power line cycle integration time. The sampling rate is 300 Hz. Two power line cycles are equal to 33.3 ms. This comes to 10 samples for each integration.

To calculate the wind-tunnel velocity, a differential pressure transducer is used to measure dynamic pressure. The transducer measures the difference between the static pressure upstream of the test section and the stagnation pressure in the room. Pressure readings are taken at 1 Hz. A correction factor is multiplied by the stagnation pressure to account for losses that occur in the tunnel inlet. Mass flow rates are measured using fixed orifice plates placed inside of the injection and suction supply ducts. Mass flow rates are calculated based on Eq. (2) [19]:

$$q_m = \frac{CE\epsilon\pi d^2\sqrt{2\rho_1 \Delta p}}{4} \tag{2}$$

where $E = 1/\sqrt{1-\beta^4}$, the pipe internal diameter $\beta = d/D$, ρ_1 is the upstream density, and Δp is the differential pressure. All values are constant except density and differential pressure. The density is found by measuring the upstream temperature and pressure. Temperature readings are taken at 1 Hz.

To calculate the total uncertainty of the mass flow rate, the square root of the sum of the squares is used as in the following equation for the mass flow rate [18]:

$$\frac{\delta q_m}{q_m} = \left[\left(\frac{\delta C}{C}\right)^2 + \left(\frac{\delta\epsilon}{\epsilon}\right)^2 + \left(\frac{2\beta^4}{1-\beta^4}\right)^2\left(\frac{\delta D}{D}\right)^2 + \left(\frac{2}{1-\beta^4}\right)^2\left(\frac{\delta d}{d}\right)^2 + \frac{1}{4}\left(\frac{\delta\Delta p}{\Delta p}\right)^2 + \frac{1}{4}\left(\frac{\delta\rho_1}{\rho_1}\right)^2\right]^{1/2} \tag{3}$$

Data in Table 1 give an uncertainty for the injection mass flow rate $\delta q_m/q_m = 0.164\%$ and for the suction mass flow rate $\delta q_m/q_m = 0.179\%$.

A Kiel probe was placed in the injection duct just downstream of the Duocel foam. This total pressure was then used to find the velocity of the injection jet. To determine the injection velocity, first the critical area ratio of a one-dimensional duct $A/A*$ is obtained by Eq. (4) [20]:

$$\frac{A}{A^*} = \frac{KP_0A_{\text{jet}}}{q_m\sqrt{T_0}} \tag{4}$$

The A/A^* can also be determined by [20]

$$\frac{A}{A^*} = \frac{1}{M}\left[\left(\frac{2}{\gamma+1}\right)\left(1+\frac{\gamma-1}{2}M^2\right)\right]^{\frac{\gamma+1}{2(\gamma-1)}} \tag{5}$$

where $K = 0.040416$, P_0 is the total pressure in the injection slot, A_{jet}

Table 1 Uncertainties for the injection mass flow rate and for the suction mass flow rate

Coefficient	Injection mass uncertainty	Suction mass uncertainty
$\frac{\delta C}{C}$	0.06	0.06
$\frac{\delta\epsilon}{\epsilon}$	0.144	0.144
$(\frac{2\beta^4}{1-\beta^4})^2(\frac{\delta D}{D})^2$	≈ 0	≈ 0
$(\frac{2}{1-\beta^4})^2(\frac{\delta d}{d})^2$	≈ 0	≈ 0
$\frac{\delta\Delta p}{\Delta p}$	0.100	0.176
$\frac{\delta\rho_1}{\rho_1} = \sqrt{(\frac{\delta p_1}{p_1})^2 + (\frac{\delta T_1}{T_1})^2}$	0.018	0.001

is the injection slot area, T_0 is the measured total temperature at the injection slot, γ has the value of 1.4. The injection jet Mach number is found by linearly interpolating the table of A/A^* and the Mach number determined by Eq. (5). The injection velocity is then calculated by the following relation:

$$V = M\sqrt{\gamma RT} \tag{6}$$

Static pressure is measured in the exit of the suction duct at the plane where the suction duct and suction manifold meet. This value is used to find the density, velocity, and total pressure in the suction duct.

The pitching moment measurement is not considered as reliable because the effect of the latex tubes is too difficult to calibrate for varying angles of attack. The pitching moment results, hence, are not presented in this paper and will be reported in the future research.

IV. Results and Discussion

The freestream Mach number is about 0.11. For the airfoil tested, this gives a Reynolds number of approximately 3.8×10^5 based on the airfoil chord, which is in the laminar/transitional region. To mimic the realistic flight conditions, the boundary layer should be turbulent. To accomplish this, the airfoil leading edge is tripped to trigger the turbulence.

Figure 3 is the comparison of the measured lift coefficients of the CFJ0025-065-196 and CFJ0025-131-196 airfoils compared with the baseline NACA0025 airfoil with different injection total pressure. For the sake of clarity, the lift coefficients of the two airfoils are plotted separately. A higher injection total pressure will yield a higher injection momentum coefficient and, hence, a higher lift coefficient and stall margin. The bottom two curves with circle and cross symbols are for the baseline NACA0025 airfoil with and without the LE trip. It shows that the tripped airfoil delays stall by about 4 deg of the AOA. This is because the fully turbulent boundary layer with the trip is more resistant to flow separation. The very bottom curve is for the CFJ airfoil without the jet on. It has a smaller stall AOA than the baseline airfoil because the steps for the injection and suction slot weaken the boundary layer and make separation occur at a smaller AOA. Overall, with the similar level of injection total pressure, the CFJ0025-131-196 airfoil has slightly higher lift than that of the CFJ0025-065-196 airfoil. The CFJ0025-065-196 airfoil with smaller injection slot size has more stall margin and, hence, higher maximum lift. Figure 3 indicates that both airfoils achieve significant lift enhancement and stall margin increments.

Figure 4 is the comparison of the injection momentum coefficient of the CFJ0025-065-196 and CFJ0025-131-196 airfoils at three different injection total pressures. The momentum coefficient is defined as

$$C_\mu = \frac{\dot{m}_j V_j}{0.5\rho_\infty U_\infty^2 S} \tag{7}$$

Here, $\dot{m}_j$ is the coflow jet mass flow rate, V_j is the injection jet velocity, and ρ_∞ and U_∞ are the freestream density and velocity, respectively. Figure 4 indicates that, with similar levels of injection total pressure, the CFJ0025-131-196 airfoil has approximately twice as large an injection mass flow rate as that of the CFJ0025-065-196 airfoil.

The power required to pump the jet is determined by the jet mass flow rate and the total pressure ratio to overcome the total pressure loss of the jet [8,9,14]. The formulation is the following:

$$P = \frac{\dot{m}_{\text{cfj}}}{\eta_{\text{cfj}}}[(PR)_{\text{cfj}}^{\frac{\gamma-1}{\gamma}} - 1] \tag{8}$$

Figure 5 is the total pressure ratio between injection and suction for the two airfoils. The figure shows that the total pressure ratio required by the CFJ0025-131-196 airfoil is significantly higher than the one required by the CFJ0025-065-196 airfoil, which has an injection slot size 50% less than that of the CFJ0025-131-196 airfoil.

The fact that The CFJ0025-131-196 airfoil has twice the mass flow rate and greater pump total pressure ratio means that the power required to pump the jet will be significantly higher than that required by the CFJ0025-065-196 airfoil. For example, Table 2 gives the comparison of the power required for the two airfoils to achieve the same lift coefficient of 4.42. The jet mass flow rate of the CFJ0025-065-196 airfoil is only half that of the CFJ0025-131-196 airfoil. Based on Eq. (8) and assuming the same efficiency for the jet pumping and recirculating system, the power to pump the CFJ0025-131-196 airfoil is then 3.9 times that needed by the CFJ0025-065-196 airfoil as shown in the table.

This example indicates that there is a large difference in power consumption (fuel consumption) by simply using different slot sizes to achieve the same lift. The airfoil configuration is not optimized in

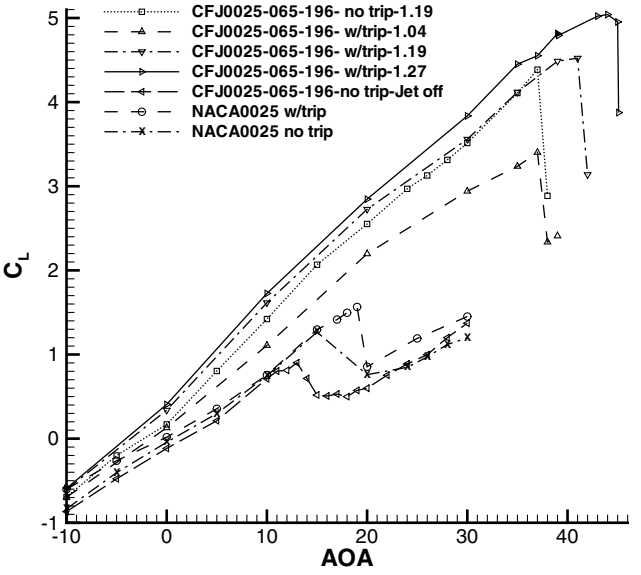

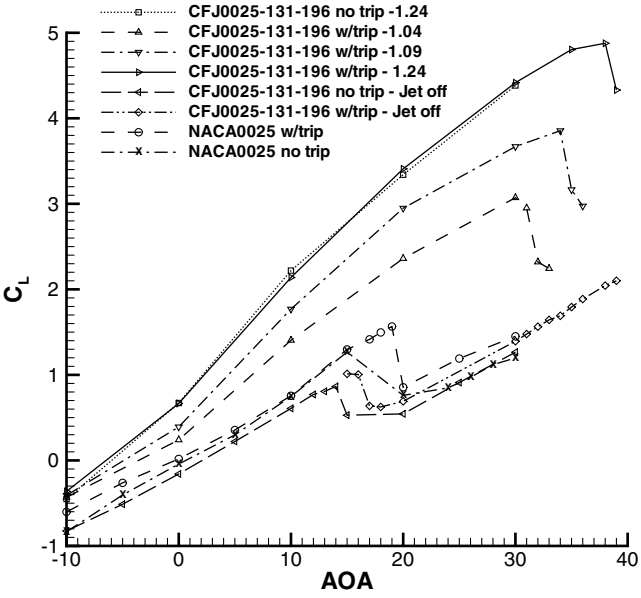

Fig. 3 Measured lift coefficients of the baseline and CFJ airfoils.

Table 2 Comparison of power required to achieve $C_L = 4.42$ for the two CFJ airfoils

Airfoil	C_L	$\dot{m}$ kg/s	PR	AOA	Power required unit
CFJ0025-065-196	4.42	0.051254	1.33	34.7 deg	1
CFJ0025-131-196	4.42	0.11	1.65	30 deg	3.9

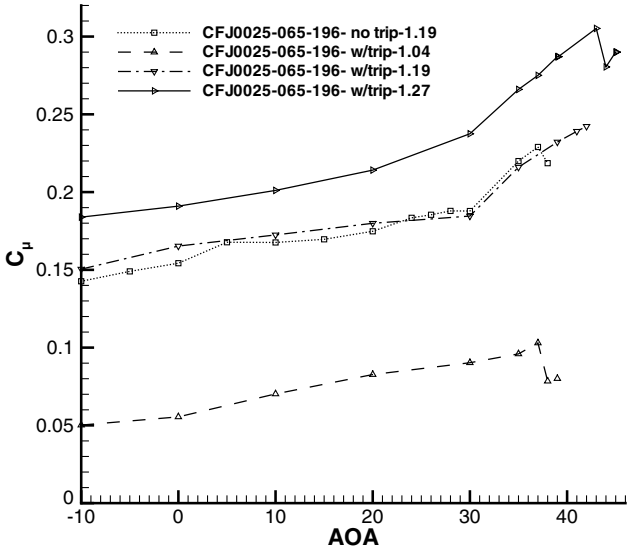

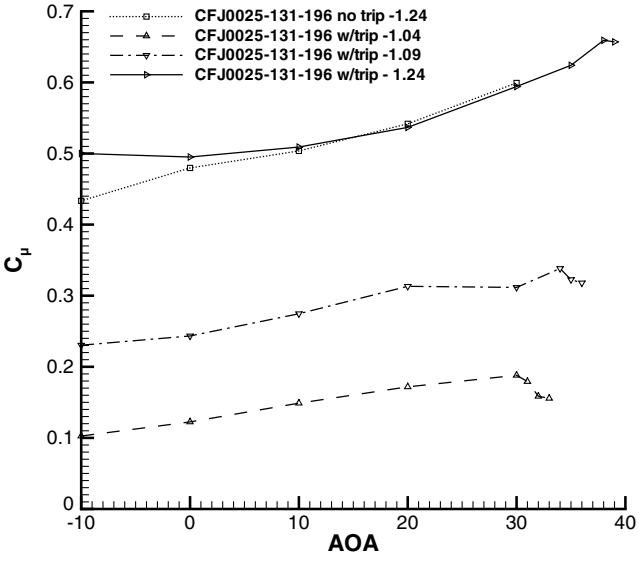

Fig. 4 Measured injection momentum coefficient of the CFJ0025-065-196 and the CFJ0025-131-196 airfoils.

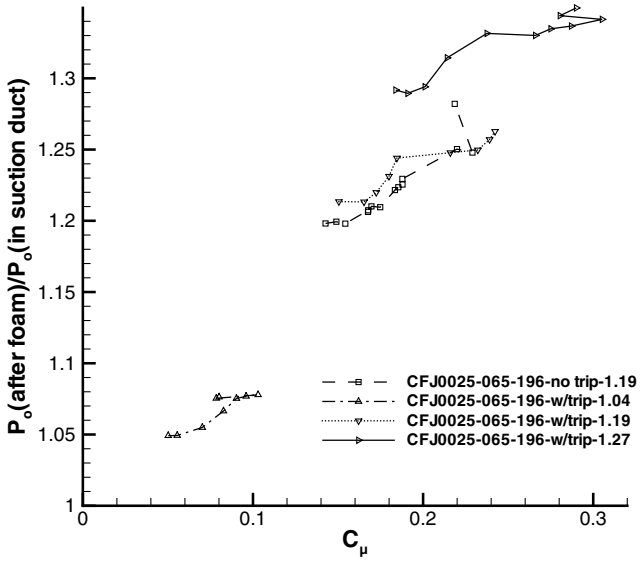

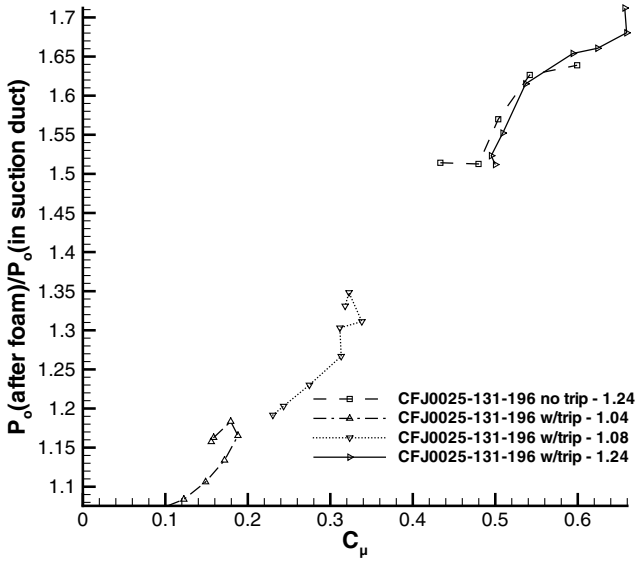

Fig. 5 Measured total pressure ratios of the two CFJ airfoils.

this study with only two slot sizes studied. This suggests that there is room for significant CFJ airfoil performance improvement if an optimum configuration study is done.

Figure 6 is the drag polar of the CFJ0025-065-196 and CFJ0025-131-196 airfoils compared with the baseline airfoil. Both the airfoils reduce the minimum drag significantly. However, the airfoil with the larger injection slot size reduces drag much more than that of the CFJ0025-065-196 airfoil as shown in Fig. 6. The negative drag (thrust) area of the CFJ0025-131-196 airfoil is substantially larger. This is the benefit associated with the airfoil with larger injection slot size.

The results summarized above indicate that, if the design purpose is to achieve high lift and high stall margin, a small injection slot should be used; if the purpose is to reduce drag, a large slot size may be preferred. There should be an optimum slot size that would be the most energy efficient, and this issue should be studied further.

It would be very useful to have a parameter that relates the injection jet geometry and the CFJ airfoil performance. Figure 7 is the ratio of the maximum lift of the two CFJ airfoils to the maximum lift of the baseline airfoil plotted against the momentum coefficient C_μ. Figure 8 is the ratio of the AOA stall margin of the two CFJ airfoils to that of the baseline airfoil again plotted against the momentum coefficient C_μ. The maximum lift and stall margin of both the airfoils correlate well with the momentum coefficient for the fixed geometry. That is, when the geometry (slot size) does not change, increasing the momentum coefficient will increase the stall margin and maximum lift coefficient. However, if all the results are viewed with different geometry (open and solid symbols), when the injection slot size varies, the test data are scattered and do not correlate well with the jet momentum coefficient. This is shown in Figs. 7 and 8.

In seeking a parameter to correlate airfoil performance that is independent of the geometry, it is found that the coefficient of jet kinetic energy per unit area appears to be suitable for $C_{L\max}$ and AOA stall margin. The coefficient of jet kinetic energy is defined as

$$C_{JK} = \frac{\rho_j V_j^2}{0.5\rho_\infty U_\infty^2} \tag{9}$$

Figure 9 is the ratio of the maximum CFJ lift of the two CFJ airfoils to the maximum lift of the baseline airfoil against C_{JK}. Figure 10 is the ratio of the AOA stall margin of the two CFJ airfoils to that of the baseline airfoil against C_{JK}. Compared with Figs. 7 and 8, the data of Figs. 9 and 10 coalesce much better and give a nearly linear trend. In general, when C_{JK} increases, the maximum lift and stall margin increase. Figures 9 and 10 indicate that, when the kinetic energy

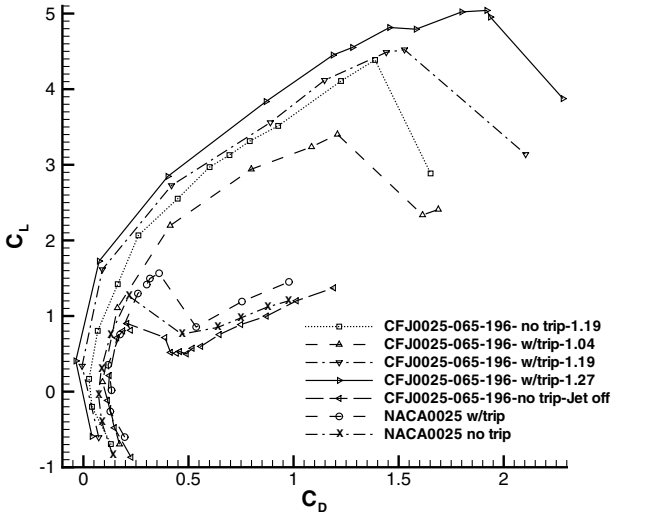

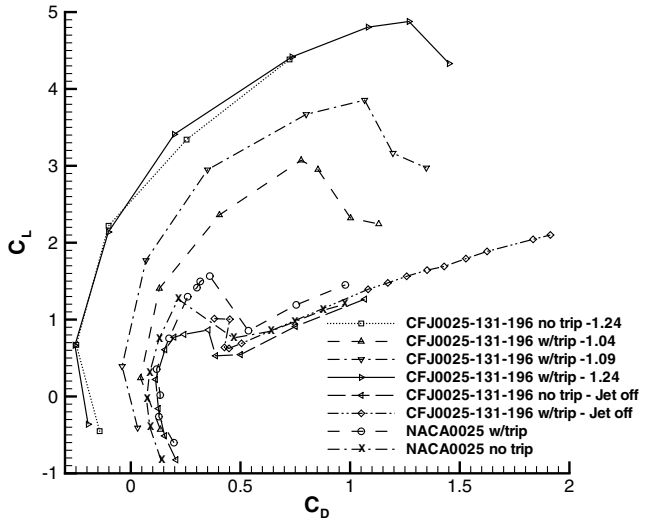

Fig. 6 Measured drag polar of the CFJ0025-065-196 and the CFJ0025-131-196 airfoils.

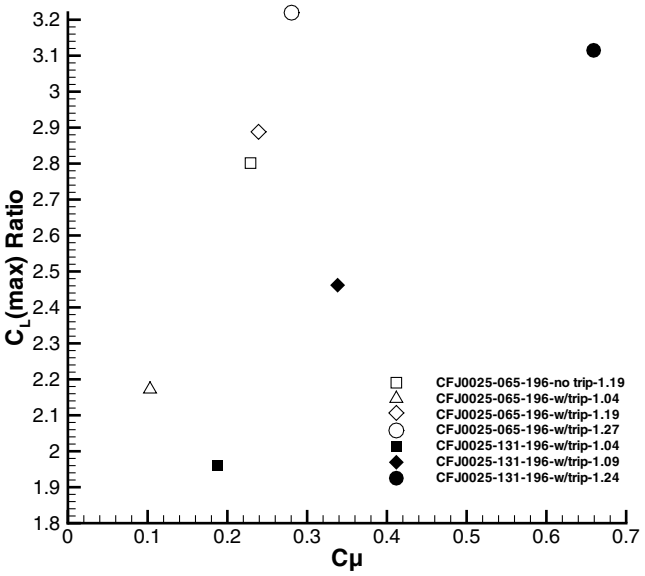

Fig. 7 Measured $C_{L\max}$ vs jet momentum coefficient for the two CFJ airfoils.

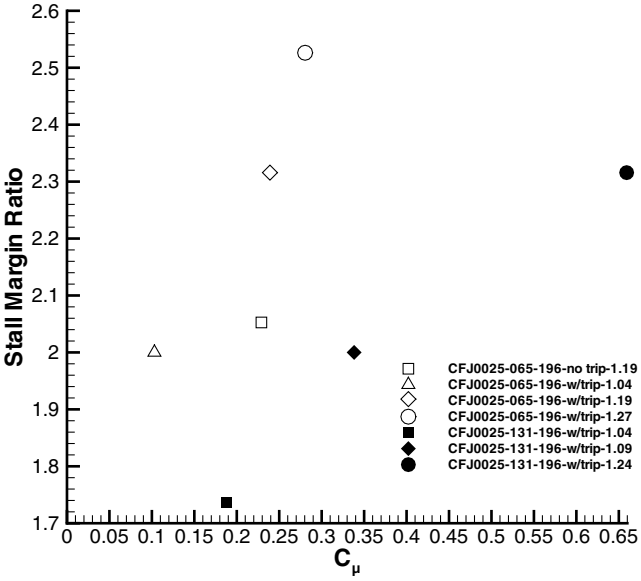

Fig. 8 Measured AOA stall margins vs jet momentum coefficient for the two CFJ airfoils.

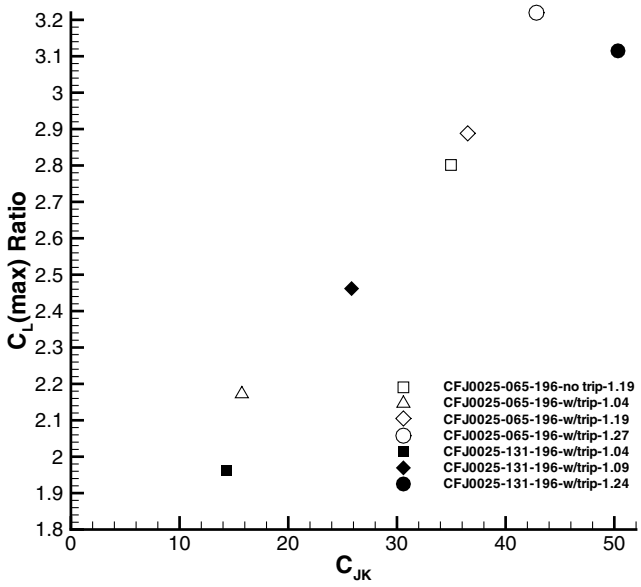

Fig. 9 Measured $C_{L\max}$ vs jet kinetic energy coefficient for the two CFJ airfoils.

coefficient varies from 14 to 50, the maximum lift of the CFJ airfoil is increased by 96 to 220%. The AOA stall margin is also increased by 74 to 153%.

For drag reduction, both the jet kinetic energy coefficient and the momentum coefficient correlate well with the test data as shown in Figs. 11 and 12. However, the momentum coefficient appears to have better linearity than the kinetic energy coefficient. The drag reduction is calculated with the minimum drag at AOA = 0 by the following formulation:

$$\text{Drag reduction} = (C_{D\,\text{cfj}} - C_{D\,\text{baseline}})/C_{D\,\text{baseline}} \qquad (10)$$

Figures 11 and 12 show that the reduction of the minimum drag of the CFJ0025-131-196 airfoil with a jet momentum coefficient of about 0.50 is 300%.

To study the effect caused entirely by the slot size, both the airfoils are tested first with the same injection total pressure coefficient $P_{0\,\text{injection}}/P_{0\,\text{freestream}} = 1.04$. Figure 13 is the lift comparison for the two airfoils. The injection total pressure coefficient is labeled in the

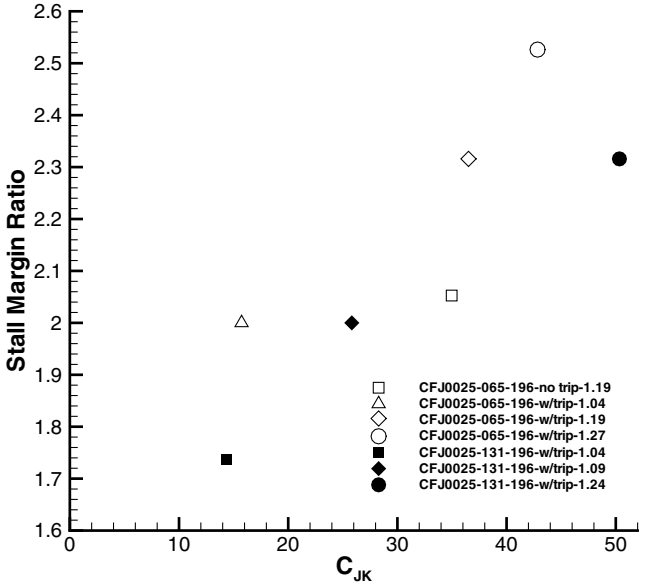

Fig. 10 Measured AOA stall margins vs jet kinetic energy coefficient for the two CJF airfoils.

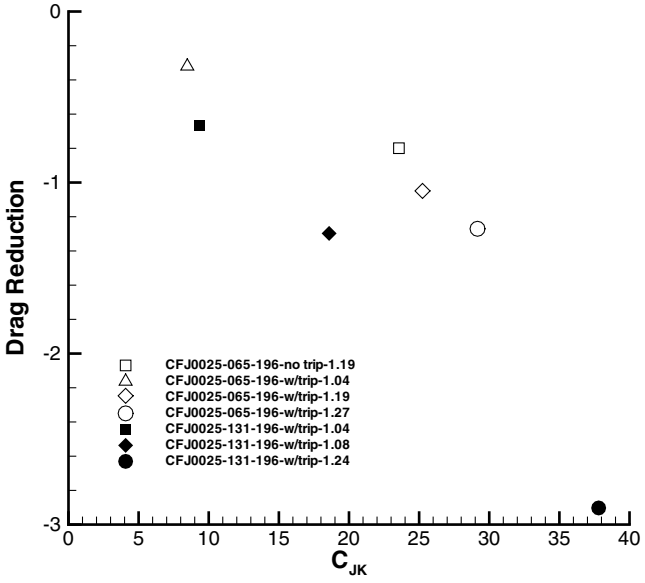

Fig. 11 Measured reduction of the minimum drag vs jet kinetic energy coefficient for the two CFJ airfoils.

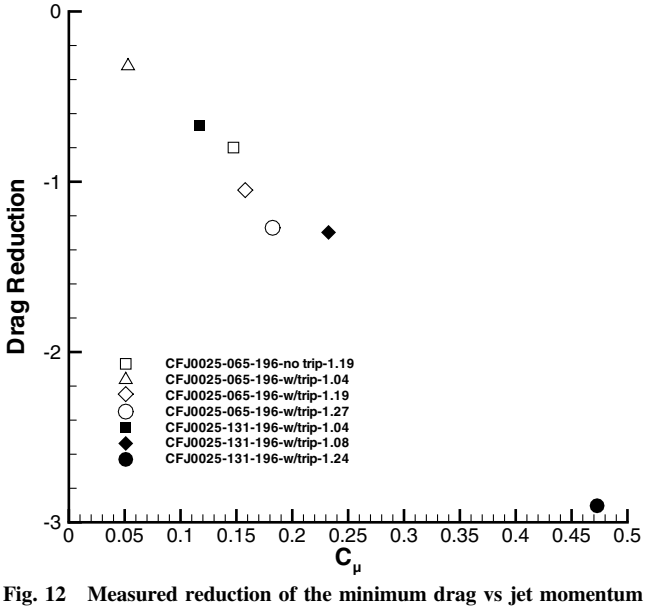

Fig. 12 Measured reduction of the minimum drag vs jet momentum coefficient for the two CFJ airfoils.

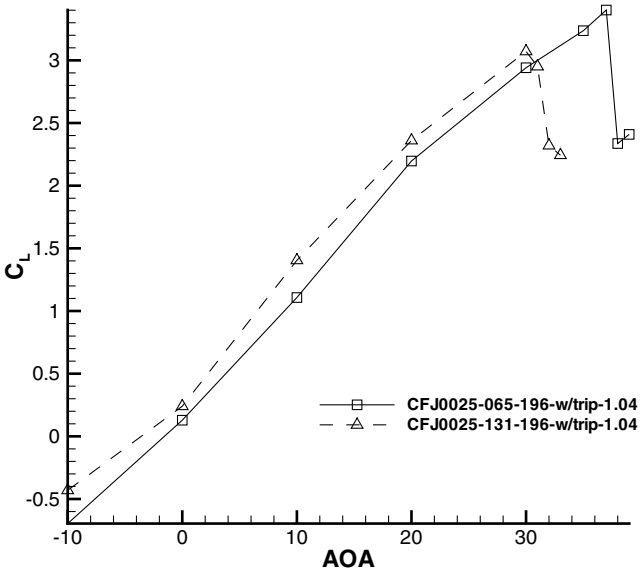

Fig. 13 Measured lift coefficients of the two CFJ airfoils with the same injection total pressure.

plot (the last number in the legend, normalized by freestream total pressure). It shows that the lift coefficient of the CFJ0025-131-196 airfoil is somewhat higher than that of the CFJ0025-065-196 airfoil before the airfoil stalls. However, the CFJ0025-131-196 airfoil stalls at an AOA $= 30$ deg, whereas the CFJ0025-065-196 airfoil with a 50% smaller injection slot size stalls at an AOA $= 36$ deg, yielding a higher maximum lift coefficient.

Figure 14 is the comparison of injection jet Mach number with the same injection total pressure, which shows that the larger injection slot size airfoil has a slightly higher jet Mach number at the same AOA before the airfoil stalls. Figure 15 is the comparison of the injection densities of the two airfoils. They are about the same and equal to the ambient density as expected in the incompressible flow regime. Figure 16 shows that the injection jet mass flow rate of the CFJ0025-131-196 airfoil is about twice as large as that of the CFJ0025-065-196 airfoil due to the larger injection slot area.

The injection mass flow rate and velocity are determined by the injection total pressure and the mainflow static pressure at the injection location. The injection total pressure is held constant while the AOA varies. When the AOA is increased, the LE suction is stronger, and the local static pressure at the injection location decreases. The injection velocity, therefore, will increase, as will the mass flow rate and the momentum coefficient as shown in Fig. 16.

Figures 13–16 indicate that the slightly higher lift of the CFJ0025-131-196 airfoil is generated by the slightly higher jet velocity, which is caused by a two times greater jet mass flow with stronger induction effect. Obviously, the price paid to gain such a small lift increase is high. Furthermore, the CFJ0025-131-196 airfoil stalls at lower AOA than the CFJ0025-065-196 airfoil even with the much larger mass flow rate. The reason for this is not fully clear at this time. It is speculated that the large centrifugal force may make the jet detach from the curved airfoil suction surface. The centrifugal force is determined by the mass flow rate, flow velocity, and surface curvature. The airfoil with the larger injection slot passes more mass flow rate and thus generates greater centrifugal force, which has the tendency to "throw" the fluid particles away from the surface.

Figure 17 is the drag comparison for the two airfoils with the same injection total pressure. The minimum drag of the CFJ0025-131-196 airfoil at AOA $= 0$ deg is about 50% lower than that of

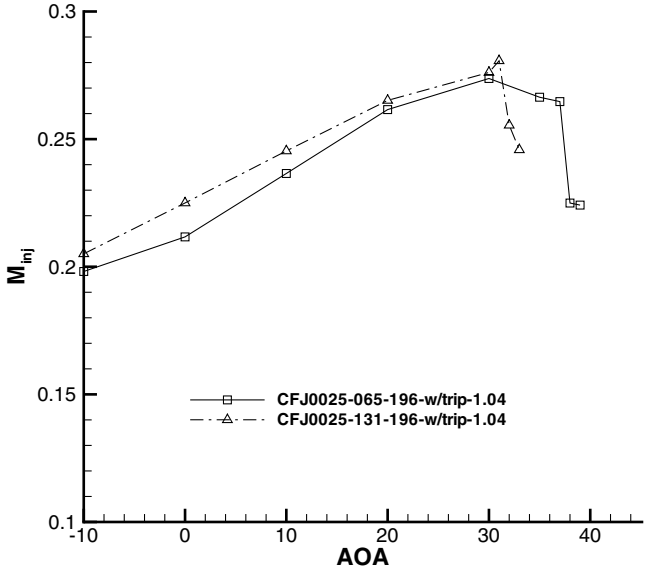

Fig. 14 Measured injection jet Mach numbers of the two CFJ airfoils with the same injection total pressure.

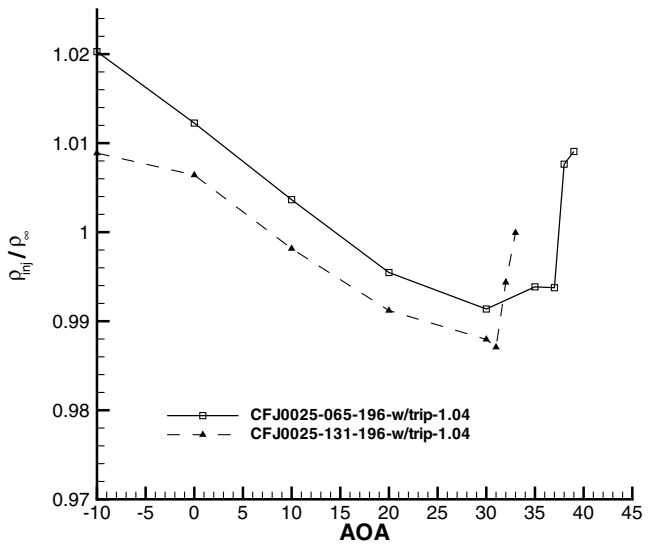

Fig. 15 Measured injection jet densities of the two CFJ airfoils with the same injection total pressure.

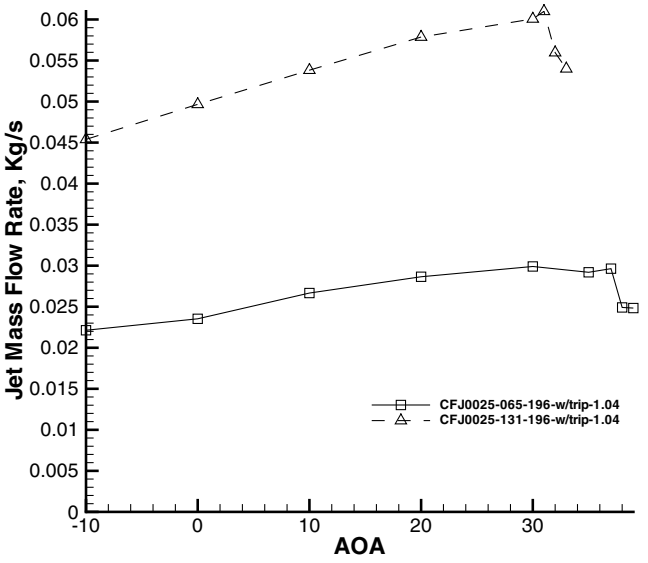

Fig. 16 Measured injection mass flow rates of the two CFJ airfoils with the same injection total pressure.

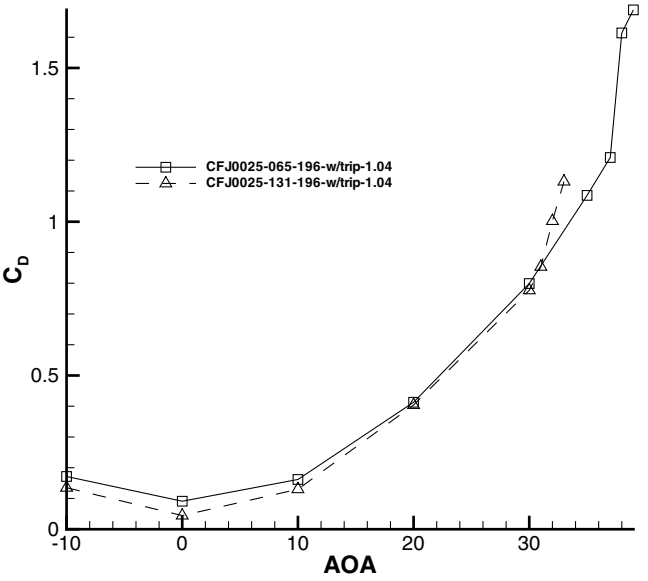

Fig. 17 Measured drag coefficients of the two CFJ airfoils with the same injection total pressure.

the CFJ0025-131-196 airfoil. The drag magnitude is determined by the airfoil wake velocity profile [8,9]. The reason that the CFJ0025-131-196 airfoil has less drag is that the jet momentum coefficient of the CFJ0025-131-196 airfoil is about twice as high due to the large jet mass flow rate. Consequently, the jet and main flow are mixed more.

V. Conclusions

Wind-tunnel tests have been conducted to investigate the effect of injection slot size for the coflow jet airfoil. Two coflow jet airfoils with injection slot size differing by a factor of 2 were tested and both demonstrate significant lift enhancement, drag reduction, and stall margin increase. With the same injection total pressure, the jet mass flow rate of the airfoil with the larger injection slot is about twice that of the smaller injection slot airfoil. At the same AOA before stall, the lift enhancement using the larger injection slot is slightly greater than the one using the smaller injection. The minimum drag reduction is more significant than the lift enhancement. The larger injection slot airfoil with higher jet mass flow rate also yields smaller stall AOA. The reason is not fully clear at this time and is speculated to be due to the centrifugal force detaching the jet. To achieve the same lift coefficient of 4.42, the power required (fuel consumption) for the larger injection slot size airfoil is 3.9 times that of the CFJ airfoil with smaller injection slot size. It appears that the smaller injection slot airfoil is more effective in increasing stall margin and maximum lift, whereas the larger injection slot airfoil is more effective in reducing drag. The two airfoils tested in this research are not optimized. The results indicate that there is a significant potential to improve the CFJ airfoil performance when an optimum configuration is found. A coefficient of jet kinetic energy is introduced, which appears to correlate better with the maximum lift and stall margin than the momentum coefficient when the CFJ airfoil slot size varies. The minimum drag reduction correlates well with both the jet kinetic energy coefficient and momentum coefficient, but the momentum coefficient has less deviation from the linear trend.

Acknowledgment

NASA LaRC is acknowledged for supporting this research under Contract No. NNL04AA39C for NRA-03-LaRC-02.

References

[1] Sellers, W. L. I., Singer, B. A., and Leavitt, L. D., "Aerodynamics for Revolutionary Air Vehicles," AIAA Paper 2004-3785, June 2003.

[2] Gad-el Hak, M., "Flow Control: The Future," *Journal of Aircraft*, Vol. 38, No. 3, 2001, pp. 402–418.

[3] Gad-el Hak, M., *Flow Control, Passive, Active, and Reactive Flow Management*, Cambridge Univ. Press, New York, 2000.

[4] Anders, S., Sellers, W. L., and Washburn, A., "Active Flow Control Activities at NASA Langley," AIAA Paper 2004-2623, June 2004.

[5] Tilmann, C. P., Kimmel, R. L., Addington, G., and Myatt, J. H., "Flow Control Research and Application at the AFRL's Air Vehicles Directorate," AIAA Paper 2004-2622, June 2004.

[6] Miller, D., and Addington, G., "Aerodynamic Flowfield Control Technologies for Highly Integrated Airframe Propulsion Flowpaths," AIAA Paper 2004-2625, June 2004.

[7] Kibens, V., and Bower, W. W., "An Overview of Active Flow Control Applications at the Boeing Company," AIAA Paper 2004-2624, June 2004.

[8] Zha, G.-C., and Paxton, C., "A Novel Airfoil Circulation Augment Flow Control Method Using Co-Flow Jet," NASA CP-2005-213509, June 2005; also AIAA Paper 2004-2208, June 2004.

[9] Zha, G.-C., Carroll, B., Paxton, C., Conley, A., and Wells, A., "High Performance Airfoil with Co-Flow Jet Flow Control," AIAA Paper 2005-1260, Jan. 2005; also *AIAA Journal* (submitted for publication).

[10] Englar, R. J., "Circulation Control for High Lift and Drag Generation on STOL Aircraft," *Journal of Aircraft*, Vol. 12, No. 5, 1975, pp. 457–463.

[11] Englar, R. J., Trobaugh, L. A., and Hemmersly, R., "STOL Potential of the Circulation Control Wing for High-Performance Aircraft," *Journal of Aircraft*, Vol. 15, No. 3, 1978, pp. 175–181.

[12] Liu, Y., Sankar, L. N., Englar, R. J., Ahuja, K. K., and Gaeta, R., "Computational Evaluation of the Steady and Pulsed Jet Effects on the Performance of a Circulation Control Wing Section," AIAA Paper 2004-0056, 2004.

[13] Wygnanski, I., "The Variables Affecting The Control Separation by Periodic Excitation," AIAA Paper 2004-2625, June 2004.

[14] Zha, G.-C., and Paxton, D. C., "A Novel Flow Control Method for Airfoil Performance Enhancement Using Co-Flow Jet," *Applications of Circulation Control Technologies*, edited by R. D. Joslin and G. S. Jones, Vol. 214, Progress in Astronautics and Aeronautics, AIAA, Reston, VA, 2006.

[15] Gao, W., Palewicz, A., Zha, G.-C., and Paxton, C. D., "Numerical Investigation of Co-Flow Jet Airfoil with Injection Only," AIAA Paper 2006-1061, 2006.

[16] Greitzer, E. M., Tan, C. S., and Graf, M. B., *Internal Flow*, Cambridge Univ. Press, New York, 2004.

[17] Zha, G.-C., Car, D., and Copenhaver, W., "Super Diffusion Cascades Using Co-Flow Jet Flow Control," National Research Council Summer Faculty Final Report, Aug. 23, 2002.

[18] Holman, J. P., *Experimental Methods for Engineers*, 7th ed., McGraw–Hill, New York, 2001.

[19] Fox, R. W., and McDonald, A. T., *Introduction to Fluid Mechanics*, 5th ed., Wiley, New York, 1998.

[20] Zucrow, M. J., and Hoffman, J. D., *Gas Dynamics*, Wiley, New York, 1976.